The Chopped Pyrgeometer: A New Step in Pyrgeometry

DIETER LORENZ AND PETER WENDLING

Institut für Physik der Atmosphäre, Deutsche Forschungsanstalt für Luft- und Raumfahrt (DLR), German Aerospace Research Establishment, Oberpfaffenhofen, Germany

PETER BURKERT, FRIEDRICH FERGG, AND GÜNTHER WILDGRUBER

SENSORLAB GmbH, Munich, Germany

(Manuscript received 2 August 1994, in final form 22 May 1995)

ABSTRACT

A new type of pyrgeometer, which uses modulation of the atmospheric radiation by a mechanical chopper, has been built for the use of ground-based and airborne measurement of broadband infrared atmospheric irradiances. The instrument basically consists of two radiometers—a target radiometer and a reference radiometer—using a specially developed chopper. The reference radiometer is used to measure the radiation of the chopper that has to be known additionally to calculate the atmospheric radiation from the signal of the target radiometer. The radiometer equations take into account the nonflat spectral response. A spectral correction factor is introduced to describe the relation between the weighted irradiance at the detector and the irradiance coming from the source. One important advantage of the chopped pyrgeometer is its nonsensitivity to the temperature distribution inside the instrument as well as its fast response.

The chopped pyrgeometer has been used during a number of airborne missions. During the Pre-EUCREX Intercomparison Campaign flown in January 1992, two Eppley pyrgeometers, two pyrgeometers of the Foot-type, and a chopped pyrgeometer were flown, in addition to other instruments on three aircraft. During a rectangular flight pattern (box) the absolute irradiance values measured by the five instruments differ by about ±10% from the average value (≈85 W m^{-2}) of all instruments, the chopped pyrgeometer indicating the smallest values throughout.

Since a detailed error budget of all instruments was not available, special emphasis was placed on relative quantities (ratios) to describe the trends measured by the various instruments along the flight tracks. It has been found that the measurements of the chopped pyrgeometer show a much better correlation to the measurement of the Foot pyrgeometers than to the Eppley instruments. A comparison of four different model calculations with the measured data of all participating instruments at ground and at three flight levels is presented.

1. Introduction

The Eppley pyrgeometer was first developed by Drummond et al. (1968) and widely used during the last 20 years to measure atmospheric irradiance in the longwave spectral region. The experience collected by the user community showed that the instrument suffers from various systematic errors, demonstrating the need to further improve the basic concept of the instrument.

For ground-based measurements it has been shown (e.g., Enz et al. 1975) that direct sunlight on the instrument caused considerable errors of the measurement. Enz (1975) reported that the error in measured irradiance may be as high as 30–120 W m^{-2} on clear days, which was found by shading the dome. Only about 7 W m^{-2} of this error accounted for direct transmission of solar radiation through the dome.

On the basis of an improved theoretical model of the instrument, Albrecht and Cox (1977) presented equations to describe the various systematic errors of the Eppley pyrgeometer. It turned out that probably the most severe problem arises from temperature differences between dome and housing, the later acting as the sink for the cold junction of the thermopile. To correct for this error, Albrecht and Cox (1977) have proposed an analytic expression assuming uniform dome temperature. In many applications, however, the dome will not be of uniform temperature and a single temperature measurement will not represent its temperature in a realistic manner. This is, for example, the case for measurements in direct sunlight, where a differential heating of the dome causes considerable errors in the order of 10% of the longwave irradiance on the ground (Alados 1988). For most aircraft observations this error is less pronounced since the strong airstream reduces local solar heating of the dome. However, nonuniform aerodynamic heating of the dome and even of the housing

Corresponding author address: Dr. Peter Wendling, Institut für Physik der Atmosphäre, DLR, 82234 Oberpfaffenhofen, Germany.

(Foot 1986) reduces the accuracy of the corresponding correction.

A further problem is to measure the sensitivity of the dome-sink temperature correction term (commonly addressed as k factor). According to Albrecht and Cox (1977) the k factor can be obtained only from a measurement far from thermal equilibrium where larger temperature differences between dome and sink are realized. This so-called dynamic calibration was applied in the laboratory as well as in the free-atmosphere during flights. The values of the k factor determined in the atmosphere may be different from those in the laboratory due to the varying influence of aerodynamics on the heat balance of the dome. Brogniez et al. (1986) suggested a generalized in-flight calibration based on inferring a relationship between the ambient physical parameters and those of the pyrgeometer heat budget. This reduces the maximum uncertainty of the measurement to 10 W m^{-2} (Brogniez et al. 1986).

Despite of all these efforts to improve the theoretical basis, calibration, and evaluation of the measurements of the Eppley pyrgeometer, the performance of the instrument was still difficult to assess, especially for aircraft applications. Foot (1986) pointed out an inconsistency in the dome-sink temperature correction caused by conduction and convective heat transport. These were not yet included in the theory of the instrument. Therefore, Foot (1986) presented a new instrument using a thermopile coated on a thin glass slide on the upper surface of the body with hot and cold junctions close together. Thus, the differential temperature of the thermopile solely depends on the radiative balance rather than on a complex heat balance of the total instrument, as in the case of the Eppley pyrgeometer. Foot (1986) compared the performance of his instrument with that of an Eppley pyrgeometer using airborne measurements and specific flight profiles where the instruments measured the same atmospheric situation several times, each time with a different thermal history. He could show that the reproducibility of his measurement is considerably better than that of the Eppley instrument, which he found to be in the order of 15 W m^{-2}. Due to the good performance of the instrument and better stabilization of the measurement after rapid thermal changes, Meteorological Research Flight (MRF) made the Foot-type instrument the standard pyrgeometer on its C-130 aircraft.

Recently Saunders et al. (1992) reported on results from an international airborne comparison experiment where, besides other instruments, Eppley pyrgeometers from different scientific groups and Foot pyrgeometers from MRF have been flown on three aircraft flying in close formation. The comparison between the Eppley pyrgeometer from the German group and the MRF instrument showed good agreement (about 3 W m^{-2}) for the downwelling irradiances but poor agreement, however, for the upwelling irradiances (about 20 W m^{-2}).

The radiometric concept of the chopped pyrgeometer is based on a completely different approach. A possibility to avoid the problems associated with radiation measurements based on modeling and measuring the heat balance of a radiometric configuration is to modulate the target radiation at the system entrance since it is state of the art in infrared radiometry. This method has the great advantage that parasitic radiation from the dome will not contribute to the radiometer signal since it is not modulated. Within this concept a special chopper for hemispherical measurement is presented and the radiation emitted by the chopper is taken into account.

2. Instrumentation

As mentioned above, the new pyrgeometer makes use of a modulation of the atmospheric radiation. Up to now choppers for the modulation were available only for a limited field of view. A chopper for modulating irradiation from a full hemisphere requires a configuration that differs from that of a plane chopper commonly used in radiometry. Two independent solutions were found by Lorenz, and the second one was selected (Lorenz 1987) based on a feasibility study (Burkert and Wildgruber 1987).

The new radiometer basically consists of two radiometers using one and the same semicylindrical 180° chopper. It is shown in Fig. 1 in perspective view, while the lower part of Fig. 1 shows a cross section of the entire radiometer. The upper radiometer measures the difference between a target radiation (atmospheric radiation or blackbody radiation in case of calibration) and the radiation from the chopper (target radiometer). The lower radiometer measures the radiation difference between an internal reference blackbody of known temperature and the chopper (reference radiometer). The purpose of the reference radiometer is to monitor the radiation of the chopper that must be known to evaluate the target radiation from the signal of the target radiometer as shown below. Due to the geometrical position of the detectors, the phase difference between the two radiometer signals is 180°. Both signals are fed to rectifiers that are synchronized by the chopper to perform a synchronous rectification. Both radiometers are equipped with pyroelectric detectors ($LiTaO_3$, diameter of flake: 2 mm) that are carrying a special black silver coating with a fairly flat spectral response throughout the infrared region. The pyroelectric detector of the target radiometer has a hemispherical field of view and is protected by a silicon dome (outer diameter 16 mm), which is coated on the inside for blocking shortwave radiation. The chopper, with a black coated inner surface, covers the dome completely during the dark phase that corresponds to a rotation of 108°. For the reference radiometer, a standard detector with a plane silicone filter and a field of view of about 60° is used. The internal reference blackbody consists of a black-coated metal surface (NEXTEL Velvet coating

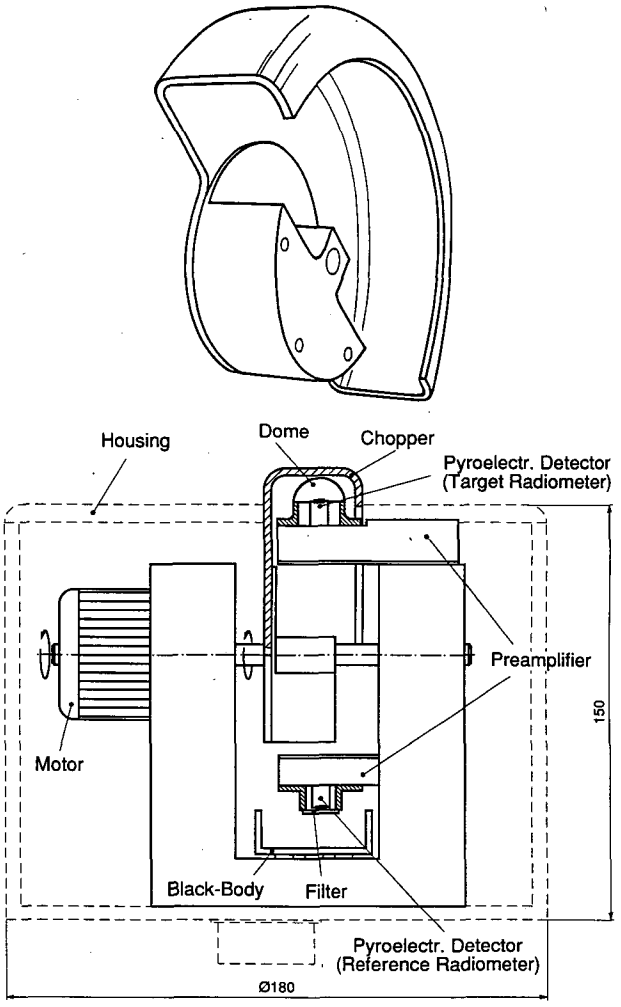

FIG. 1. Upper—perspective view of the semicylindrical chopper. Lower—setup of the chopped pyrgeometer.

2010) and a PT 100 temperature sensor. All surfaces inside the housing affecting the detectors are coated with the same black color. Since the responsivity of pyroelectric detectors is a function of the flake temperature, the temperature of the detector is monitored to correct the electrical signal. The temperature coefficient of the individual detector is measured in the laboratory. Depending on the type of pyroelectric detector, temperature coefficients (relative signal change per kelvin) between 400 and 1000 ppm K^{-1} have been observed.

Several other temperatures within the instrument are measured for housekeeping purposes. The instrument is protected by a cylindrical housing of aluminum. On the aircraft the instrument is connected to the fuselage via a special flange that contains the electrical connections.

The major electronic stages for signal conditioning and synchronous rectification are shown in Fig. 2. The chopping frequency is stabilized to 12 Hz. The position of the chopper is monitored by two sensors, one provides a reference angle and the other generates one hundred pulses per revolution (see Fig. 2). The signals of both pyroelectric detectors are fed to preamplifiers and buffer amplifiers, both providing a total amplification of approximately 700 for the target detector and 2300 for the reference detector. After the preamplifier the dc components are filtered out by a first-order high-pass filter with a corner frequency 0.023 Hz. All other signal conditioning stages, data acquisition, and instrument control electronics are mounted in a rack that is connected to the pyrgeometer head.

The thermal time constant of the pyroelectric detectors results in a signal decay during each half period of the chopper phase (Fig. 2b). To avoid second-order errors in subsequent stages induced by timing jitter, this decay is compensated by an integrator, which is reset once per chopper revolution to avoid saturation caused by integrator long-term drifts. The compensation is done in the laboratory by monitoring the signal with an oscilloscope and trimming the integration time constant until the signal plateau is horizontal (Fig. 2b). The compensated signal is fed into a voltage-to-frequency converter, with a subsequent counter that is enabled at a specific chopper position and then allowed to count for a predefined time interval (10 ms). The counter produces two "integrals" n_+ and n_- for the chopper "completely open" phase and the chopper "completely closed" phase, respectively (Fig. 2b), which are stored for each chopper period along with housekeeping data for subsequent off-line analysis. The equivalent of a synchronous demodulation is done numerically by software (Fig. 2b).

3. Radiometric equations

The following arguments and equations are formulated assuming that the spectral responsivity of the detectors is independent of wavelength, the directional response of the radiometers follows the cosine law, and the filtered irradiances are constant over the sensitive areas of the detectors. These assumptions are an usual and good approximation to the real measurement situation.

The output voltage of a chopped radiometer is proportional to the difference of the two irradiances observed on its detector area in the course of one chopping cycle. Applying this to the target radiometer (index 1) and the reference radiometer (index 2), one can write

$$U_1 = c_1(T_1)r_1(E_{\theta_1,\mathrm{TAR}} - E_{\theta_1,\mathrm{CHO}}) \qquad (1a)$$

$$U_2 = c_2(T_2)r_2(E_{\theta_2,\mathrm{REF}} - E_{\theta_2,\mathrm{CHO}}), \qquad (1b)$$

where U_i is the dc output of radiometer i, r_i is the instrumental constant at a reference temperature T_0, r_i

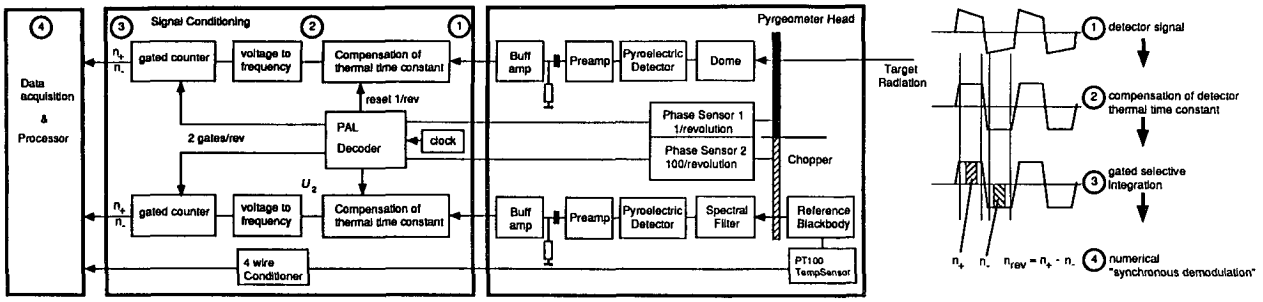

FIG. 2. (a) Block diagram of the chopped pyrgeometer (left). (b) Signal condition steps (right).

is the responsivity of detector i including the electronics amplification, multiplied by the detector area, $c_i(T_i)$ is the temperature correction factor of r_i, and $E_{\theta_{i,j}}$ is the "filtered" irradiance observed on the sensitive area of detector i, where j denotes the source of irradiance: j = TAR, CHO, REF, corresponding to target, chopper, internal reference blackbody.

The radiometric properties of the pyrgeometer subsystems may be clarified by analyzing the quantity $E_{\theta_{i,j}}$:

$$E_{\theta_{i,j}} = \int_0^\infty \theta_i(\lambda) \int_{\Omega_i} L_{i,j}(\lambda, \vartheta, \varphi) \cos(\vartheta) d\omega d\lambda$$

$$= \int_0^\infty \theta_i(\lambda) E_{i,j}(\lambda) d\lambda, \quad (2)$$

where $\theta_i(\lambda)$ is the spectral transmittance of the dome ($i = 1$) and of the plane filter, respectively, ($i = 2$), $L_{i,j}(\lambda, \vartheta, \varphi)$ is the spectral radiance of the source j as seen by radiometer i, where in general $L_{i,j}$ depends on ϑ, φ with ϑ the elevation angle and φ the azimuth with respect to the detector area, Ω_i is the solid angle as seen from detector i, and $E_{i,j}(\lambda) = \int_{\Omega_i} L_{i,j} \cos(\vartheta) d\omega$ is the unfiltered spectral irradiance for the general case.

In the case of field measurement, $L_{1,\mathrm{TAR}}$ is the radiance of the atmosphere that generally is anisotropic. The other three radiances $L_{i,j\neq\mathrm{TAR}}$, however, are emitted by surfaces inside the instrument being coated with diffuse black laquer. These emitting areas exhibit a high emissivity $\epsilon \geq 0.95$ (Lohrengel 1987) and are in radiative equilibrium with surrounding surfaces of approximately the same temperature. Thus, one may assume that $L_{i,j\neq\mathrm{TAR}}$ is an isotropic blackbody radiance B_λ.

Therefore, for $j \neq$ TAR one can modify (2):

$$E_{\theta_{i,j=\mathrm{TAR}}} = \int_0^\infty \theta_{i,}(\lambda) \int_{\Omega_i} B_{\lambda,j} \cos(\vartheta) d\omega d\lambda$$

$$= \Omega_i^P \int \theta_i(\lambda) B_{\lambda,j} d\lambda, \quad (3)$$

with $\Omega_i^P = \int_{\Omega_i} \cos(\vartheta) d\omega$ the projected solid angle as seen by detector i.

Due to the hemispherical field of view of the target radiometer, $\Omega_1^P = \pi$, whereas $\Omega_2^P < \pi$ due to the restricted field of view of the reference detector. Here

$$E_{i,j\neq\mathrm{TAR}}(\lambda) = \Omega_i^P B_{\lambda,j} \quad (4)$$

is the unfiltered spectral irradiance in the case of $j \neq$ TAR. Equation (4) is also valid for $j =$ TAR in the specific case of calibration when radiometer 1 receives the irradiance from a black cavity radiator (section 4).

In order to transform (1a) and (1b) into the radiometric equations of the two radiometers, one has to substitute the filtered irradiances $E_{\theta_{i,j}}$ by the corresponding unfiltered irradiances $E_{i,j}$. For that the following spectral correction factors are defined for atmospheric radiation:

$$\eta_{1,\mathrm{TAR}} = n_1 \frac{E_{1,\mathrm{TAR}}}{E_{\theta_{1,\mathrm{TAR}}}} = n_1 \frac{\int_0^\infty E_{1,\mathrm{TAR}}(\lambda) d\lambda}{\int_0^\infty \theta_1(\lambda) E_{1,\mathrm{TAR}}(\lambda) d\lambda}, \quad (4a)$$

and for radiation inside the pyrgeometer:

$$\eta_{i,B,j} = n_i \frac{E_{i,j\neq\mathrm{TAR}}}{E_{\theta_{i,j=\mathrm{TAR}}}} = n_i \frac{\int_0^\infty B_{\lambda,j}(T) d\lambda}{\int_0^\infty \theta_i(\lambda) B_{\lambda,j}(T) d\lambda}. \quad (4b)$$

In Eqs. (4a) and (4b) the terms n_i are defined as

$$n_i := \frac{\int_0^\infty \theta_i(\lambda) B_\lambda(T_0) d\lambda}{\int_0^\infty B_\lambda(T_0) d\lambda} \quad (4c)$$

with $T_0 = 300$ K.

In order to derive the spectral correction factor $\eta_{1,\mathrm{TAR}}$, one has to calculate the spectral irradiance $E_{1,\mathrm{TAR}}(\lambda)$ of the atmosphere by using atmospheric simulation models. Correspondingly, the calculations of $\eta_{i,B,j}$ are carried out by use of the Planck formula.

Substituting the filtered irradiances in (1a) and (1b) and introducing the spectral correction factors leads to the radiometric equations of the pyrgeometer:

$$U_1 = R_1 c_1(T_1)\left(\frac{E_{1,\mathrm{TAR}}}{\eta_{1,\mathrm{TAR}}} - \frac{\Omega_1^P B_{\mathrm{CHO}}}{\eta_{1,B,\mathrm{CHO}}}\right) \quad (5a)$$

$$U_2 = R_2 c_2(T_2)\left(\frac{\Omega_2^P B_{\mathrm{REF}}}{\eta_{2,B,\mathrm{REF}}} - \frac{\Omega_2^P B_{\mathrm{CHO}}}{\eta_{2,B,\mathrm{CHO}}}\right), \quad (5b)$$

with $R_i = n_i r_i$

$$B_j = \int_0^\infty B_{\lambda,j}\, d\lambda.$$

Contrary to r_i in (1a) and (1b), the instrumental constants R_i in (5a) and (5b) depend on the spectral transmittances of the dome of the target radiometer and the plane filter of the reference radiometer, respectively.

Due to the procedures of calibration (section 4), it is convenient to substitute R_2 by q, with

$$q = \frac{R_1 \Omega_1^P}{R_2 \Omega_2^P} = \frac{R_1 \pi}{R_2 \Omega_2^P}$$

and to rewrite (5b):

$$U_2 = c_2 \pi \frac{R_1}{q}\left(\frac{B_{\mathrm{REF}}}{\eta_{2,B,\mathrm{REF}}} - \frac{B_{\mathrm{CHO}}}{\eta_{2,B,\mathrm{CHO}}}\right). \quad (5c)$$

Solving (5a) and (5c) for $E_{1,\mathrm{TAR}}$ leads to

$$E_{1,\mathrm{TAR}} = \eta_{1,\mathrm{TAR}}\left[\frac{U_1}{c_1(T_1)R_1} - \frac{lqU_2}{c_2(T_2)R_1} + \frac{l\pi B_{\mathrm{REF}}}{\eta_{2,B,\mathrm{REF}}}\right], \quad (6)$$

with $l = \eta_{2,B,\mathrm{CHO}}/\eta_{1,B,\mathrm{CHO}}$.

The quantities of the right-hand side of (6) are derived in the following way:

(a) the constants R_1 and q are calibrated with the procedures described in section 4;

(b) the functions $c_1(T)$ and $c_2(T)$ are determined by means of temperature tests carried out with each of the detector–preamplifier units;

(c) during measurement the pyrgeometer delivers the outputs U_1, U_2, T_1, T_2, and T_{REF}; and

(d) the spectral correction factors $\eta_{1,\mathrm{TAR}}$ and $\eta_{i,B,j}$ are computed numerically as shown in section 5.

4. Calibration

For evaluation of the radiometer measurements, the quantities q and R_1 must be calibrated. In practice it is convenient to determine the quantity q without knowledge of R_1. Contrarily, for the evaluation of R_1 the value of q must be known.

For the determination of q one can take advantage of the status of the pyrgeometer in a quiet laboratory environment, where all signals usually remain constant with time. Under such steady-state conditions the chopper is cooled down by less than 10° (e.g., with the help of a standard "cooling spray"). As soon as cooling stops the chopper warms up again, so that the signals U_1 and U_2 change, whereas all other signals remain constant; q may then be deduced from the rate of change of U_1 and U_2.

Assuming $E_{1,\mathrm{TAR}}$, T_1, T_2, T_{REF} to be constant, one can differentiate U_1 with respect to time in (5a):

$$\frac{d}{dt}U_1 = -c_1 R_1 \pi \frac{d}{dt}\left(\frac{B_{\mathrm{CHO}}}{\eta_{1,B,\mathrm{CHO}}}\right). \quad (7)$$

Within the temperature range of 10° around room temperature all correction factors $\eta_{i,B,\mathrm{CHO}}$ deviate from the average value by not more than 10^{-2} (see Fig. 7) so that $\eta_{1,B,\mathrm{CHO}}$ may be regarded as constant. Therefore (7) may be approximated by

$$\frac{d}{dt}U_1 \approx \frac{-c_1 R_1 \pi}{\eta_{1,B,\mathrm{CHO}}}\frac{d}{dt}B_{\mathrm{CHO}}. \quad (8a)$$

Similarly, one can differentiate U_2 in (5c) and obtain

$$\frac{d}{dt}U_2 \approx \frac{-c_2 R_1 \pi}{q\eta_{2,B,\mathrm{CHO}}}\frac{d}{dt}B_{\mathrm{CHO}}. \quad (8b)$$

The ratio of (8a) and (8b) results in

$$\left(\frac{dU_1}{dt}\right)\left(\frac{dU_2}{dt}\right)^{-1} = q\frac{c_1\eta_{2,B,\mathrm{CHO}}}{c_2\eta_{1,B,\mathrm{CHO}}} = Z. \quad (9)$$

In (9) all quantities except q are known.

In practice q was evaluated by linear regression. It can easily be shown that (9) is equivalent to the following expression where U_1 appears as a linear function of U_2:

$$U_1(t) = A + ZU_2(t), \quad (10a)$$

with $U_1(t)$, $U_2(t)$ being the pyrgeometer outputs at the same time. Terms A and Z are constants, with Z being defined in (9).

Substituting Z and rearranging the terms in (10a) leads to

$$\frac{c_2}{c_1}U_1 = \frac{c_2}{c_1}A + q\frac{\eta_{2,B,\mathrm{CHO}}}{\eta_{1,B,\mathrm{CHO}}}U_2. \quad (10b)$$

The linear regression is applied to (10b), where q is the slope of the linear function between the variables (c_2U_1/c_1) and $(\eta_{2,B,\mathrm{CHO}}U_2/\eta_{1,B,\mathrm{CHO}})$. Figure 3 shows an example based on a measurement with a pyrgeometer that was equipped with a dome of the same spectral type as used with the Eppley pyrgeometers and with a filter of pure silicon in the reference radiometer.

For the calibration of R_1, the pyrgeometer measures the isotropic irradiance of a blackbody source by looking into a black cavity that covers the hemispherical field of view of the target radiometer. In the course of a calibration cycle, the temperature T_{cal} of the calibration source is varied in a wide range. Here R_1 is deduced by linear regression after transforming (6) into

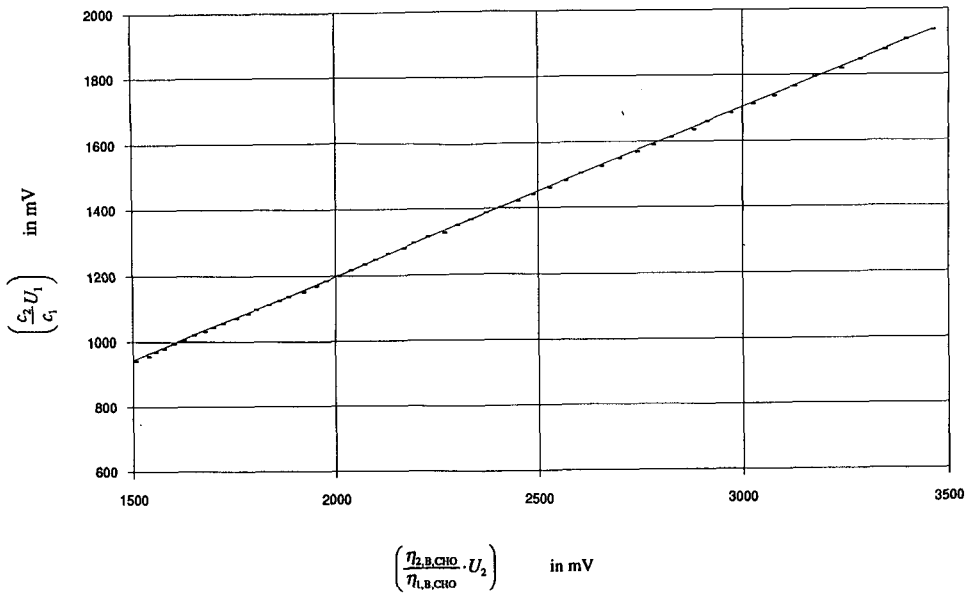

FIG. 3. Example of measured data illustrating the evaluation of q on basis of Eq. (10b). Here q is the slope of the straight line that is the least squares fit to the data points; the result is $q = 0.51$. The measurement was carried out with a chopped pyrgeometer being equipped with a dome of the same spectral type as used with the Eppley pyrgeometer. As experienced with various pyrgeometers (i.e., equipped with various domes with different coatings and detectors), the range of q is $0.40 < q < 0.60$.

$$\frac{U_1}{c_1} - I\frac{U_2}{c_2}q = R_1\left(\frac{E_{1,\mathrm{TAR}}}{\eta_{1,\mathrm{TAR}}} - I\frac{\pi B_{\mathrm{REF}}}{\eta_{2,B,\mathrm{REF}}}\right), \quad (11)$$

with $E_{1,\mathrm{TAR}} = \pi B_1(T_{\mathrm{cal}})$ and $\eta_{1,\mathrm{TAR}} = \eta_{1,B,\mathrm{cal}}$.

The left-hand side of (11) is a linear function of the term in brackets on the right-hand side and R_1 is the slope of the straight line. In Fig. 4 an example for a calibration cycle is given.

5. Spectral correction

In the past many pyrgeometer measurements have been evaluated assuming a flat spectral response of the instrument. As mentioned above, the domes of most of the modern pyrgeometers are fabricated from silicon with a coating for solar blocking. Silicon, however, shows considerable absorption features in some regions above 6 μm. Additional absorption is caused by the coating. Therefore, a spectral correction of the measurements is necessary. Foot (1986) has shown that in case of blackbody radiation at temperatures between 246 and 300 K, such a correction is as low as 1.4%. For atmospheric radiation he calculates differences of up to 6 W m^{-2} between flat and dome filtered measurements. Based on these results, Kilsby and Foot (1991) developed a correction formula that leads to an additive correction term.

The correction factor $\eta_{1,\mathrm{TAR}}$ as introduced in this paper [see Eq. (4a)] can be written

$$\eta_{1,\mathrm{TAR}} = \frac{\int_0^\infty \theta_1(\lambda)B_\lambda(T_0)d\lambda}{\int_0^\infty B_\lambda(T_0)d\lambda} \times \frac{\int_0^\infty\int_0^{2\pi} L_{1,j=\mathrm{atm}}(\lambda,\omega)\cos\vartheta d\omega d\lambda}{\int_0^\infty\int_0^{2\pi} \theta_1(\lambda)L_{1,j=\mathrm{atm}}(\lambda,\omega)\cos\vartheta d\omega d\lambda}. \quad (12)$$

From this equation two facts become evident.

(a) The term $\eta_{1,\mathrm{TAR}}$ depends on the spectral as well as on the directional distribution of the atmospheric radiation.

(b) For the determination of $\eta_{1,\mathrm{TAR}}$, the knowledge of the relative distribution of the spectral response $\theta_1(\lambda)$ is sufficient. This can be seen when one substitutes $\theta_1(\lambda)$ by [const $\times\ \theta_1(\lambda)$], which does not change the value of $\eta_{1,\mathrm{TAR}}$. In the same way $\eta_{i,B,j}$ can be described by use of (4b), where the directional distribution of $B_{\lambda,j}(T)$ has to be isotropic.

The definition of n_i causes the $\eta_{i,B,j}$ to become equal to unity when the correction is applied to the Planck radiation at a temperature of $T = T_0$. For $\eta_{1,\mathrm{TAR}}$ this is true only for the case of isotropic Planck irradiance as applied during calibration.

The correction factors for three types of domes with different spectral transmittances were investigated. These

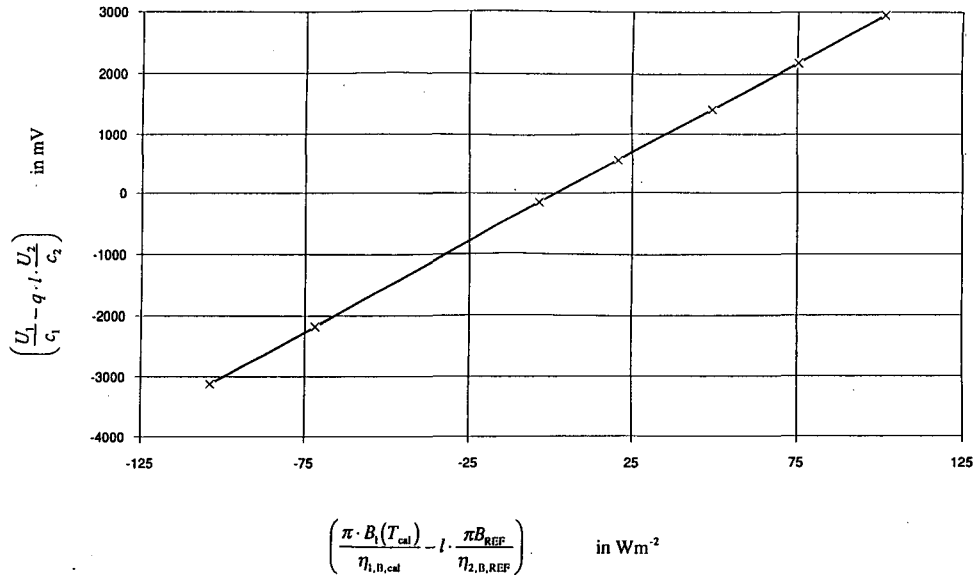

FIG. 4. Example of measured data illustrating the evaluation of R_1 on the basis of Eq. (11). Here R_1 is the slope of the straight line that is the least squares fit to the data points; the result is $R_1 = 31.2$ mV (W m^{-2})$^{-1}$. The measurement was carried out with the same pyrgeometer as with Fig. 3. As experienced with various pyrgeometers the range of R_1 is $25 < R_1 < 40$ mV (W m^{-2})$^{-1}$.

transmission curves are shown in Fig. 5 in the reduced spectral resolution as they were used for the numerical calculations. The first curve is that of uncoated silicon with a cut-on at 1 μm, which does not suppress sun radiation. Therefore, it is used as a window for the detector of the reference radiometer. It was also used for the dome of the target radiometer in case of night measurements. There are two relevant advantages. First, such a dome has a uniform transmittance across the entire surface. Second, it can serve as a reference for coated silicon domes.

The curve as denoted by 2 is that of a silicon dome with an interference coating being typical for Eppley and Foot pyrgeometers. It has a steep cut-on between 3 and 4 μm and a transmission in some spectral regions

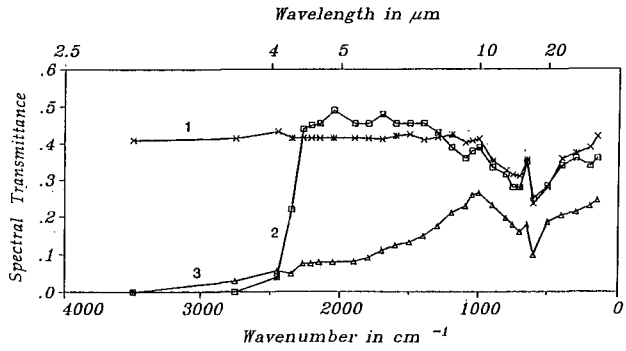

FIG. 5. Spectral transmittance of three different types of domes that have been used for the chopped pyrgeometer: 1) uncoated silicon (Si); 2) silicon dome with interference coating (Reading); 3) silicon dome with absorption coating (OIB K7).

that is higher than that of uncoated silicon. In general, the problem with these domes is that the coating is not uniform across the surface. Therefore, a further dome coating was investigated. This has an absorption coating that is homogeneous across its surface. Compared to the interference coatings, the cut-on is not as steep and the transmission is lower. It seems that this coating is the best choice because there are good chances to improve absorption coatings in the future.

The calculations of $\eta_{1,\mathrm{TAR}}$ and $\eta_{i,B,j}$ were performed for these three domes. Two model atmospheres typical for cloudless midlatitude summer and winter situations were used to determine $\eta_{1,\mathrm{TAR}}$ at different levels between ground and an altitude of 45 km. These calculations were carried out by applying a radiative transfer model based on the matrix operator theory of Plass et al. (1973) and for which the computer code was developed and described by Grassl (1987). For determination of $\eta_{i,B,j}$, the Planck formula was used.

All calculations were done by use of a computer code limited to the wavelength range between 4 and 200 μm. This limitation was found to cause only negligible errors.

The resulting correction factors are shown in Figs. 6 and 7 as function of different variables in the abscissas. These are helpful for the practical data evaluation according to (6) for which $\eta_{1,\mathrm{TAR}}$ is needed versus $E_{\theta_1,\mathrm{TAR}}/n_1$ or $\eta_{1,B}$ versus B_{θ_1}/n_1 (Fig. 6) and $\eta_{1,B,\mathrm{CHO}}$, as well as $\eta_{2,B,\mathrm{CHO}}$ versus temperature T (Fig. 7). Figure 6 shows that $\eta_{1,\mathrm{TAR}}$ differs insignificantly for both cloudless atmospheric models as long as the value of $E_{\theta_1,\mathrm{TAR}}/n_1$ is greater than 25 W m^{-2}, corresponding to

an altitude of about 12 km. This implies that at least for these situations the special atmospheric situations can be neglected. More important is that there is a considerable difference between $\eta_{1,\mathrm{TAR}}$ and $\eta_{i,B,j}$. This difference implies that uncertainties arise in atmospheric situations where there is a mixture of clear and cloudy sky (cloud irradiation can be considered to be similar to that of a diffuse blackbody). These uncertainties are relevant for measurements of the downward-directed flux with scattered or broken clouds. The same problem arises when one measures the upward-directed flux from high altitudes. In these cases the pyrgeometer always receives a mixture of blackbody and atmospheric irradiance. Currently one has to assess for an uncertainty of ±2% in such cases. This uncertainty is not a problem specific to the chopped pyrgeometer but is common to all pyrgeometers with silicon domes.

Improvements of the coatings, as well as further investigations of the correction factors, are under way. The results presented in Fig. 6 show that the correction factors $\eta_{1,\mathrm{TAR}}$ and $\eta_{i,B,j}$ lead to a significant improvement even when the actual spectral and directional distribution of the atmospheric irradiance is not known.

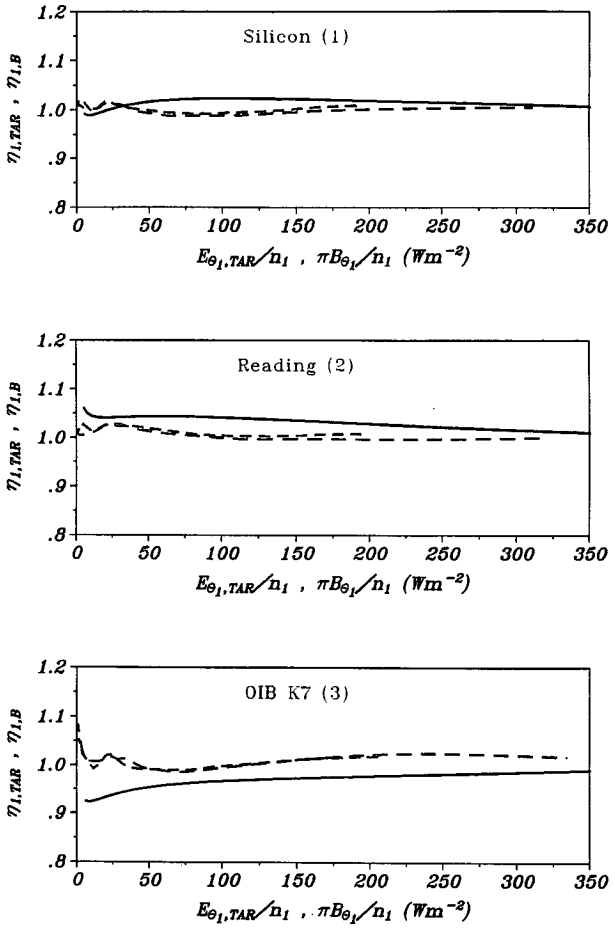

FIG. 6. Spectral correction factors for three types of domes as explained in Fig. 5 and three different sources: blackbody (solid curve), midlatitude summer atmosphere (long dashes), and midlatitude winter (short dashes).

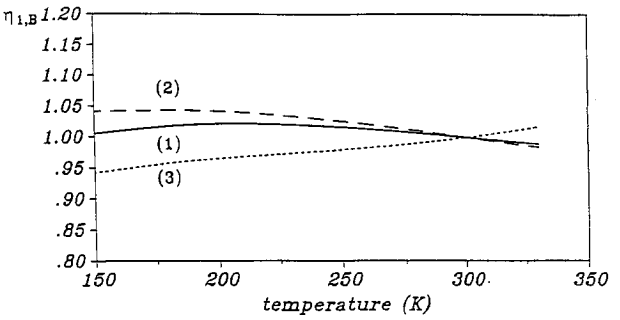

FIG. 7. Spectral correction factors for three types of domes as explained in Fig. 5 for a blackbody source.

6. Measurements

The new pyrgeometer was tested on the ground and during numerous aircraft campaigns with the DLR meteorological research aircraft "Falcon." As an example, results are presented from the Pre-EUCREX Intercomparison Campaign, which took place between 21 and 23 January 1992 off the southwestern peninsula of England. Three aircraft were involved in the campaign: the C-130 of the U.K. Meteorological Office (Meteorological Research Flight, MRF), the Merlin IV of the French Météorologie Nationale, and the Falcon-E of the German Deutsche Forschungsanstalt für Luft- und Raumfahrt (DLR). Shortwave and longwave broadband irradiances were measured using sets of standard Eppley pyranometers and pyrgeometers on board the Falcon and the Merlin, one set looking up and one set looking down. The C-130 was also equipped with standard Eppley pyranometers, whereas the pyrgeometers used were those developed by Foot (1986). Two upward-looking Foot pyrgeometers were flown: these are referred to subsequently as MRF-1 and MRF-2. In addition to that, the Falcon carried an upward-looking chopped pyrgeometer mounted on the top of the fuselage. The aim of the campaign was to compare the results of the different types of instruments under various atmospheric and flight conditions. In order to measure the same target at the same time, a part of the flight program was devoted to flights in close formation of the three aircraft. A part of the data from this campaign will be used in the following to demonstrate the performance of the chopped pyrgeometer and to compare it with that of the other pyrgeometers.

The details of calibration and data evaluation, including corrections for the Eppley pyrgeometers as well as for the Foot pyrgeometers, have been described by Saunders et al. (1992). The spectral transmission of the dome was taken into account by applying a correction according to Kilsby and Foot (1991) to the Eppley

TABLE 1. Time and flight data taken from Falcon data record for the 10-s average irradiance samples at the start and end of the legs of the flight box. The altitude for legs A to D was 6.1 km.

	Time (UTC)	Latitude (°N)	Longitude (°E)	Heading (°)	Temperature (°C)
Start leg A	1320:10	50.94	−3.86	191	−24.0
End leg A	1325:10	50.54	−4.02	191	−23.3
Start leg B	1327:00	50.47	−4.18	283	−24.2
End leg B	1331:20	50.5	−4.71	282	−22.9
Start leg C	1333:50	50.61	−4.84	13	−22.6
End leg C	1338:00	50.88	−4.77	13	−22.7
Start leg D	1340:00	50.92	−4.62	106	−22.6
End leg D	1345:10	50.77	−4.08	106	−24.4

and Foot pyrgeometer measurements. The Eppley pyrgeometers on board the Merlin were operated by Laboratoire d'Optique Atmosphérique, Universite des Sciences et Technique de Lille (LOA). The chopped pyrgeometer was equipped with a dome type 3 (see Fig. 5).

For instrument comparison, data were taken from those phases of the flight where the three aircraft flew in a close formation side by side, and consequently, all the instruments measured the same target. In principle, an error may occur due to a different orientation of the instruments with respect to the vertical. However, data taken during curves within the flight-box show that at least under the atmospheric conditions of the considered comparison, attitude changes in the order of 5° produce a negligible change in measured downward irradiance. Therefore, slight errors in the orientation of the instruments can probably be neglected in the analysis of the data of the flight legs.

A boxlike pattern was flown with the aircraft separated a few tens of meters at an altitude of approximately 6.1 km with partly cloudless sky above flight level. The four sides of the box are called leg A to leg D, the flight starting with leg A. Table 1 shows the flight data (Falcon dataset) at the beginning and at the end of the time intervals that have been used for data analysis. The measured downward irradiance (averages over 1 s) of all five instruments for legs A and B is shown in Fig. 8. Along leg A all measurements indicate a fairly constant irradiance level. The measured values of all instruments lie within a band of about ±10% of the average value of about 85 W m^{-2}. Along leg B all instruments indicate an increase of the downward irradiance on the order of 4%, which might be caused by a thin cirrus layer above flight level. If one looks at the trend that the various instruments measured along the legs, it can be seen that they differ slightly in describing this trend. To show this more clearly, the ratios of the various measurements are shown in Fig. 9. These ratios suppress all ambient irradiance changes and therefore make it possible to get an impression of the stability of the instruments involved in the comparison. To get a qualitative statement for the stability of the

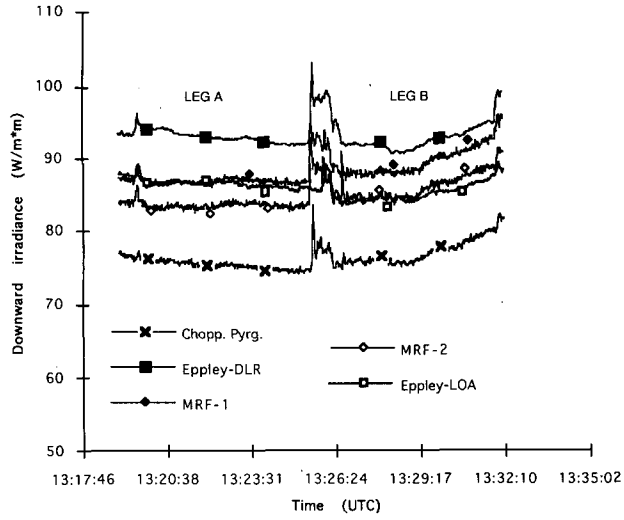

FIG. 8. Downward longwave irradiance as measured by five different pyrgeometers along legs A and B.

chopped pyrgeometer, its measurement was ratioed to the two Eppley pyrgeometers and to the two Foot pyrgeometers. If the chopped pyrgeometer would be subject to signal instabilities or drifts that are greater than those of the other instruments, then all ratios with the chopped pyrgeometer would show a similar trend. This, however, is not the case, as can be seen from the ratios in both legs. Therefore, it is evident that the stability of the chopped pyrgeometer is at least on the order of the stability of the other instruments.

The irradiances measured along legs C and D generally show a behavior similar to those along legs A and B. The irradiances of the box show approximately

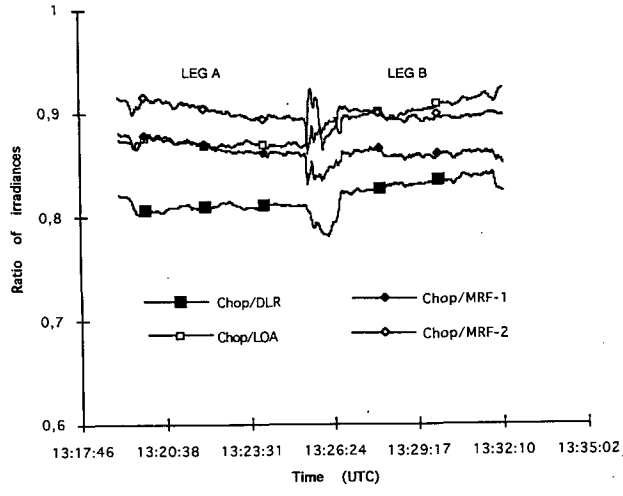

FIG. 9. Ratios of measured irradiances of different instruments along legs A and B: 10-s running average; ratio between the chopped pyrgeometer values and those of two Eppley instruments (DLR and LOA) and two Foot pyrgeometers.

constant values along legs A and C and for legs B and D increasing or decreasing values, respectively. A summary of the data of all four legs is shown in Figs. 10a,b. Each leg is described by five equidistant samples of signal averages over 10 s. The trends the various instruments indicated along the legs are very similar. The French Eppley shows some features in legs C and D that are not indicated by the other instruments. On the other hand, the changes from leg to leg differ considerably for the various instruments. This is evident, for example, from leg B to C and from leg C to D, where the French Eppley indicates a change that differs substantially from that measured by the other instruments. A similar result can be seen for the German Eppley pyrgeometer from legs C to D. This behavior may result from different sensitivity of the various instruments to a change in flight conditions or solar azimuth. Generally one can expect that the change of the measured irradiance between the end of a leg and the start of the following leg (the positions do not differ more than about 10 km) is small compared to the changes observed along leg B or D. However, the measurements do not show this behavior (Fig. 10a).

As a summary of the results for the flight box, the ratios of the chopped pyrgeometer measurements to all other instruments are shown in Fig. 10b. Leaving aside for the moment the fact that all the ratios are significantly less than 1, which indicates that the chopped pyrgeometer is measuring less than all other the instruments, the information from these data is twofold. First, any errors that are due solely to differences in the calibration of each of the instruments will result in ratios that are constant for all samples of the box pattern but that will be offset from each other. Second, any sensitivity that the instruments have to changing measurement conditions (e.g., instrument temperature, solar azimuth, etc.) will be shown by changes in the ratios during the series of measurements. This case is observed, for example, in the ratios of chopped pyrgeometer to LOA Eppley and chopped pyrgeometer to DLR Eppley from leg C to leg D (opposite change of ratios). This could indicate a changing sensitivity of the two instruments between legs C and D, resulting from the different conditions encountered during these legs. If the ratios change along one leg (as it is the case for leg B for the same two ratios as just mentioned), the instruments differ in describing the trend of irradiances along this leg, as already discussed above. From the data of all four legs it can be seen that the change of the ratios is in most cases larger between two legs than along the legs, which is a further indication of a different sensitivity of each instrument type to changing conditions between the legs. Further, the data in Fig. 10b clearly indicate a much better correlation between the measurements of the chopped pyrgeometer to those of the Foot-type instruments than to the measurements of the Eppley pyrgeometers. The comparison to the ratio between the two Foot-type instruments further shows that

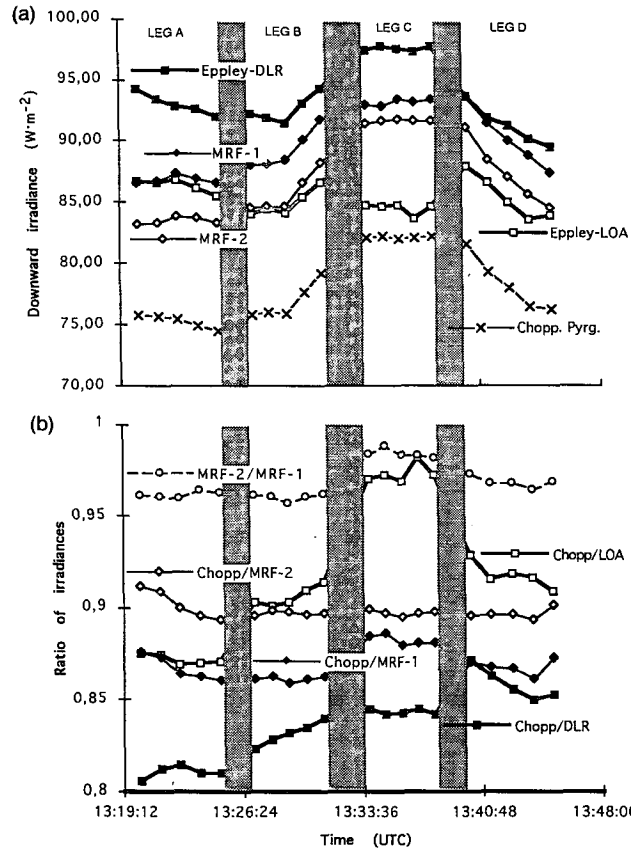

FIG. 10. (a) Samples (10-s average) of measured irradiance along legs A to D. The samples are shown by symbols that are connected by straight lines for quick identification. (b) Ratio of measured irradiance samples of (a); ratio between the chopped pyrgeometer values and those of two Eppley instruments (DLR and LOA) and two Foot pyrgeometers; also shown is the ratio between the two Foot pyrgeometers for comparison.

the correlation between the measurements of the chopped pyrgeometer to those of the Foot-type instruments is as good as the correlation between the measurements of the two Foot-type instruments. These findings demonstrate that the stability of the chopped pyrgeometer is at least comparable to that of the Foot-type instruments, which was demonstrated to be better than those of the Eppley pyrgeometers (Foot 1986).

A comparison of measured and calculated downwelling longwave irradiances is given in Table 2. For this purpose different radiation schemes were used that have been described by Saunders et al. (1992) and by Shine (1991) (MRF Shine model). In addition to the coordinated aircraft measurements shown in Figs. 8, 9, and 10, the measurements of the Falcon at a height of 10.7 km and of all three aircraft at 0.9 km and on ground are included in Table 2. At the height of 10.7 km no plausible values of the DLR Eppley are available. The irradiance measured by the chopped pyrgeometer is well within the range predicted by the various

TABLE 2. Results from the Pre-EUCREX intercomparison flight of January 1992. Model calculations refer to a cloudless atmosphere.

	Pyrgeometer measurements					Model calculations			
Height (km MSL)	MRF-1	MRF-2	Eppley LOA	Eppley DLR	Chopped Pyrgeom.	MRF Roach-Slingo	MRF Shine	Univ. Lille LOA	DLR Meerkötter
10.70	—	—	—	0 to −30	26 (23–29)	30	24	23	26
6.1	86.8 (86.5–87.4)	83.5 (83.2–83.9)	86.3 (85.5–86.8)	92.9 (91.9–94.1)	75.3 (74.4–75.8)	90	80	86	76
6.1	89.3 (88.0–91.7)	85.7 (84.6–88.2)	84.9 (83.9–86.6)	92.5 (91.3–94.2)	76.9 (75.7–79.1)	90	80	86	76
6.1	93.1 (92.7–93.3)	91.6 (91.3–91.7)	84.4 (83.6–84.7)	97.4 (97.2–97.65)	82.1 (82.0–82.2)	90	80	86	76
6.1	90.2 (87.3–93.6)	87.3 (91.0–84.5)	85.3 (83.5–87.8)	91.2 (89.4–93.5)	78.3 (76.2–81.5)	90	80	86	76
0.9	219	222	—	207	(198–206)	195	187	196	193
0.07 (ground)	239	238	—	235	221	223	218	226	217

Comments: All irradiance data in watts per square meter.
Data at altitude 6.1 km: first value is the average, values in parentheses indicate minimum and maximum of 10-s averages given in Fig. 7a.

models. At the level of 6.1 km, the influence of clouds has to be considered. The model calculations refer to a clear-sky atmosphere, whereas the measurements at least of the later parts of the legs at 6.1 km were disturbed by high thin clouds. Therefore, only the lowest measured values can be compared to the calculations. These values show that the measurement of all instruments lie within a range (75.3–92.9 W m^{-2}) consistent with the range given by the various models. A different situation can be found at 0.9 km and at ground. Here the measured irradiances of the nonmodulated instruments are significantly higher than the model predictions, whereas the values given by the chopped pyrgeometer lie within the range given by the models. The discussion of the table shows that pyrgeometer measurements from an aircraft and their interpretation is very difficult. More confidence in the absolute measurement can probably be established only by comparing the performance of all instruments on the basis of standardized laboratory procedures, thus deriving error limits for each instrument, which are valid for clearly defined measurement conditions.

The error of the measurement has been estimated for the chopped pyrgeometer, assuming reasonable errors for the various instrument parameters (e.g., output voltages, the temperature of the internal blackbody, temperature coefficient of detectors) that have to be used to calculate the measured irradiance. The calculation includes the calibration process since the calibration will cause a canceling of some systematic errors of the instrument parameters to a first order. The rms errors of the measurement for the three flight levels given in Table 2 are 1.9 W m^{-2} (0.9 km), 2.8 W m^{-2} (6.1 km), and 3.2 W m^{-2} (10.7 km). A more detailed error analysis including errors due to spectral correction is in preparation.

7. Conclusions

A new chopped pyrgeometer has been designed based on the well-established technique of radiation modulation that is state of the art in infrared systems. The problem of chopping a detector with a hemispherical field of view has been solved by designing a chopper with a special geometry. The radiation of the blackened chopper that must be known for the evaluation of the measurement is measured with a second radiometer that uses the same chopper. The radiometric equations of the instrument show that the accuracy of the measurement will not be affected by the thermal condition of the instrument. This is the main advantage compared to pyrgeometers, which are based on the measurement of the radiative balance of a thermopile, like the Eppley pyrgeometers.

During the Pre-EUCREX Intercomparison Campaign in January 1992 the chopped pyrgeometer could be compared to Eppley and Foot-type pyrgeometers. The data of a flight box pattern have been analyzed for this work. During this flight section, the three aircraft carrying the instruments were flown in close formation side by side. Thus, all the instruments essentially measured the same target. The downward irradiances measured by the various instruments in the flight box lie within a band of about ±10% of the measured average value of 85 W m^{-2}, the chopped pyrgeometer always indicating the lowest levels of all instruments. When compared to the average of calculations using different models, the measurements of the chopped pyrgeometer show the best agreement of all pyrgeometers. Looking at the irradiance ratios between the various instruments and the chopped pyrgeometer, it was found that the ratio between the chopped pyrgeometer and the two Foot-type pyrgeometers shows the smallest changes (<3%). The corresponding changes for the Eppley instruments are about 6% (DLR) and 9% (LOA).

The reasons for the considerable differences in the measured irradiance values between the various instruments have not been analyzed in detail. This would require a detailed error analysis of all instruments, including spectral correction applied for the domes, errors due to deviations from the cosine law, and possible calibration errors. Unfortunately most of these data

were not available for this work. A preliminary error estimate for the chopped pyrgeometer considering the influence of various instrument parameters yields an rms error of 2.8 W m^{-2} for an irradiance level of 75 W m^{-2}. The error estimate does not include possible errors caused by insufficient spectral correction or a deviation from the cosine characteristic, each of which may be higher than the other systematic errors of the instrument.

The ideal pyrgeometer has a completely flat spectral response and an exact cosine characteristic. Any real instrument will provide these characteristics only to some extent. To enable a better quantitative comparison of measurements of various pyrgeometers, further effort should focus on modeling and measuring all those performance parameters that have to be known to correctly interpret the measurement.

Acknowledgments. The authors are greatly indebted to DLR for funding the development of the chopped pyrgeometer. It is gratefully acknowledged that Dr. G. Brogniez from Laboratoire d'Optique Atmospherique, Universite des Sciences et Technique de Lille and Dr. P. Francis from Meteorological Research Flight, U.K. Meteorological Office put their data at our disposal and supported our work with helpful discussions. Without their results, a comparison of the chopped pyrgeometer with the state of the art would not have been possible. The authors thank Dr. R. Meerkötter and W. Thomas from DLR for calculating the spectral correction factors, and H. Fimpel for support data evaluation. We further thank Dr. K. Dehne from the Meteorological Observatory Hamburg for helpful discussions. In addition, the excellent work of the DLR flight facility and data management group that contributed to the success of the campaign is acknowledged.

REFERENCES

Alados-Arboledas, L., J. Vida, and J. I. Jiménez, 1988: Effects of solar radiation on the performance of pyrgeometers with silicon domes. *J. Atmos. Oceanic Technol.*, **5,** 666–670.

Albrecht, B., and S. K. Cox, 1977: Procedures for improving pyrgeometer performance. *J. Appl. Meteor.*, **16,** 188–197.

Brogniez, G., J. C. Buriez, J. C. Vanhoutte, and Y. Fouquart, 1986: An improvement of the calibration of the Eppley pyrgeometer for the case of airborne measurements. *Contrib. Atmos. Phys.*, **59,** 538–551.

Burkert, P., and G. Wildgruber, 1987: Studie über die Realisierbarkeit eines neuartigen Wechsellichtradiometers zur Messung der aus dem Halbraum kommenden Strahlung, im Auftrag der DLR, Nr. 5-553-8335. [Available from DLR-PA, D-82230 Wessling, Germany.]

Drummond, A. J., W. J. Scholes, J. M. Brown, and R. E. Nelson, 1968: A new approach to the measurement of terrestrical longwave radiation. WMO Tech. Note, **104,** 383–387.

Enz, J. W., J. C. Klink, and D. G. Baker, 1975: Solar radiation effects on pyrgeometer performance. *J. Appl. Meteor.*, **14,** 1297–1302.

Foot, J. S., 1986: A new pyrgeometer. *J. Atmos. Oceanic Technol.*, **3,** 363–370.

Grassl, H., 1978: Strahlung in getrübten Atmosphären und Wolken. Hamburger Geophysikalische Einzelschriften No. 37, 135 pp.

Kilsby, C. G., and J. S. Foot, 1991: Pyrgeometer corrections due to dome transmission. M.R.F. Tech. Note No. 3, Farnborough, Hunts.

Lohrengel, J., 1987: Gesamtemissionsgrad von Schwärzen. *Wärme-u. Stoffübertragung,* **21,** 311–315.

Lorenz, D., 1987: Einrichtung zur Messung der aus dem Halbraum kommenden elektromagnetischen Strahlung (Electromagnetic Radiation Detection Device with Hallow Semicylindrical Chopper). Patent Germany (priority 12 March 1987), No. 3.708.043, 29 December 1988; Europe No. 0.282.029, 9 September 1992; United States No. 4.873.433, 10 October 1989; Canada, No. 1.310.506, 24 November 1992; Japan, March 1994.

Plass, G. N., G. W. Kattawar, and F. E. Catchings, 1973: Matrix operator theory of radiative transfer. Part I: Rayleigh scattering. *Appl. Opt.*, **12,** 314–329.

Saunders, R. W., G. Brogniez, J. C. Buriez, R. Meerkötter, and P. Wendling, 1992: A comparison of measured and modeled broadband fluxes from aircraft data during the ICE '89 Field Experiment. *J. Atmos. Oceanic Technol.*, **9,** 391–406.

Shine, K. P., 1991: On the cause of the relative greenhouse strength of gases such as the halocarbons. *J. Atmos. Sci.*, **48,** 1513–1518.